Compact Selective Bandpass Filter With Wide Stopband for TETRA Band Applications

Vinay Kumar Killamsetty, *Student Member, IEEE,* and Biswajeet Mukherjee, *Senior Member, IEEE*

***Abstract*— A selective miniaturized bandpass filter with wide stopband for TETRA band applications is presented in this paper. Basic resonator used in the filter construction is an open stub-loaded-short-circuited stepped-impedance resonator, which has the inherent property of having harmonics far from the fundamental mode. The high selectivity of the filter is obtained by virtue of the transmission zeros around the passband. The transmission zeros are generated because of the mixed electric and magnetic coupling between the resonators and the feedline structures. The selective filter has a miniaturized size of $0.078\lambda_g \times 0.082\lambda_g$ with a wide stopband extended up to 4.91 times the operating frequency.**

***Index Terms*— Bandpass filter, compact, mixed coupling, selectivity, wide stopband.**

I. Introduction

INCREASE in the number of wireless applications sharing the same electromagnetic (EM) spectrum has created the need for bandpass filter with high selectivity, wide stopband, and compact size. Many researchers have reported different ways of designing a bandpass filter. However, very few methods were useful in designing a miniaturized filter with high selectivity and wide stopband.

The basic exploration of designing a bandpass filter started with quarter-wavelength parallel-coupled line (PCL) filter [1], which has the disadvantage of large size and presence of repeated harmonics. In order to eliminate these drawbacks, modifications were made to introduce wiggly and fractal-shaped lines as in [2] and [3], respectively, to suppress harmonics. Similarly, stepped-impedance lines were used in [4] to reduce the size and to suppress the harmonics. In [5], it has been reported that the use of asymmetric stepped-impedance coupled lines in place of uniform symmetric coupled lines can reduce size and suppress harmonics. To reduce the size of the PCLs, a new design called hairpin filter is introduced in [6], where the straight lines in PCL were bent in the shape of a hairpin. Though the size is reduced by using this technique, the problems like harmonics and low selectivity still existed. In [7], open-loop resonators arranged in cross-coupled configuration were used to generate a pair of transmission zeros around passband, and in [8], open-loop resonators with open-circuit stubs were used to obtain wide stopband. In place of multiple resonators, some researchers reported the use of single-loop resonators in [9]–[11]. In [9], a square loop resonator with open-loop elements connected at corners is proposed. In [10], a miniaturized square loop resonator with an inductive perturbation at a corner has been employed, whereas a miniaturized, dual-mode ring constructed with quasi-lumped inductors and interdigital capacitors is made use of in [11]. Though the circuit size is reduced by using these techniques, the selectivity and stopband performance of the filters are still poor. Metamaterial is used in [12] to design a compact filter. Cross-coupled trisection stepped-impedance resonators (SIRs) in [13], hexagonal SIRs in [14], mixed-coupled SIRs in [15], and spiral SIRs in [16] are used to achieve compact filter. Some other novel structures that have been employed are meander-line resonators [17], hybrid resonators with interdigital coupled lines [18], [19], short-circuited triangular resonant cells [20], triangular stub-loaded short-circuited resonators [21], and parallel feeding technique [22] for designing compact bandpass filters. An alternative method of attaching series of shunted parallel and series resonant resonators along a transmission line was employed in [23] to achieve selective bandpass filter response.

In this paper, a miniaturized, selective, and wide stopband bandpass filter is designed using open stub-loaded-short-circuited stepped-impedance resonator (OSL-SCSIR). The resonator makes the filter very compact. The four resonators used in construction of the filter are arranged in a way, to create EM coupling between them. The open stub in the OSL-SCSIR aids in tuning the electric coupling strength between the resonators. This EM coupling helps in achieving transmission zeros around the passband. The source–load coupling deployed between the input–output feeding transformers helps in achieving additional transmission zero. The proposed filter is designed and simulated using CST Microwave Studio software, which is based on finite-integration technique. Design model is solved using frequency domain solver with hexahedral meshing by keeping 40 mesh cells per wavelength.

Fabrication is done by manual photolithography etching process on Rogers RO3010 substrate having the properties: $\epsilon_r = 10.2$, dielectric thickness $= 1.28$ mm, metal thickness $=$ 0.017 mm, and $\tan\delta = 0.0022$.

II. Resonator Analysis

The schematic layout of the proposed filter is shown in Fig. 1(a). It is composed of four OSL-SCSIRs (R_1, R_2, R_3, and R_4) and two impedance transformer (IT) lines connected to 50-Ω feedlines. The proposed resonator with dimensions

Manuscript received November 17, 2017; accepted January 11, 2018. Recommended for publication by Associate Editor T. Wu upon evaluation of reviewers' comments. *(Corresponding author: Vinay Kumar Killamsetty.)*

The authors are with the Department of Electronics and Communication Engineering, Indian Institute of Information Technology, Design and Manufacturing, Jabalpur 482005, India (e-mail: email2vkk@gmail.com; biswajeet.26@gmail.com).

Color versions of one or more of the figures in this paper are available online at http://ieeexplore.ieee.org.

Digital Object Identifier 10.1109/TCPMT.2018.2803218

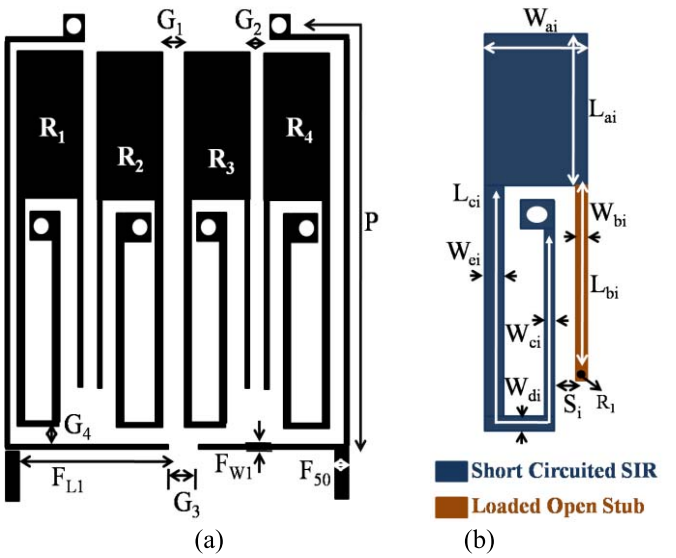

Fig. 1. (a) Schematic view of the proposed bandpass filter. (b) Structure of the OSL-SCSIR with dimensions.

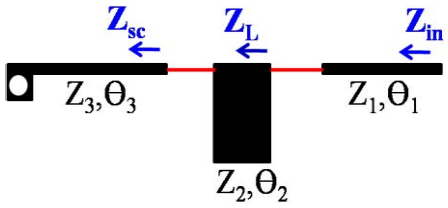

Fig. 2. Transmission line model of the OSL-SCSIR.

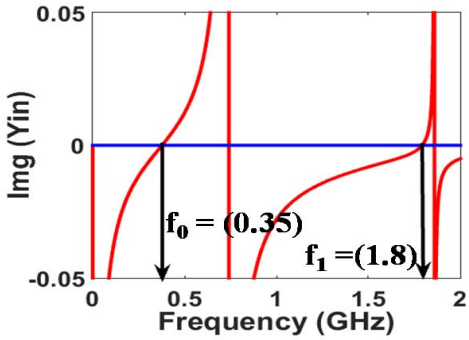

Fig. 3. Modes of the OSL-SCSIR.

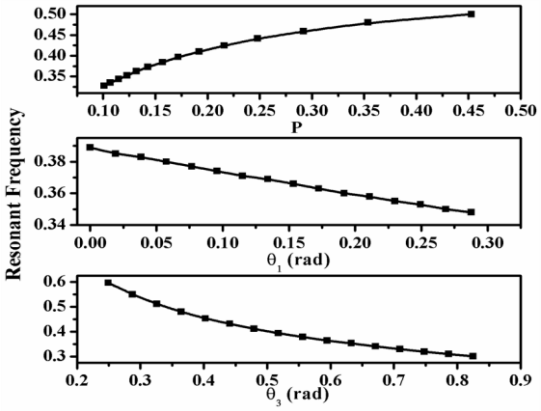

Fig. 4. Variation in fundamental mode resonant frequency position with dimensions.

can be seen in Fig. 1(b). Each OSL-SCIR is constructed by appending an open stub with an SCSIR. The resonant modes of the resonator can be obtained from the input admittance of the resonator.

The input admittance of the resonator is calculated from the transmission line model of the OSL-SCSIR shown in Fig. 2. As the resonator is composed of three sections, namely, short-circuited line, a thick transmission line, and a thin open stub cascaded in line, input impedance is derived at the end of each section to find out overall input impedance Z_{in}. Input admittance is found by reciprocating input impedance

$$Z_{\text{SC}} = jZ_3 \tan\theta_3 \tag{1}$$

$$Z_L = jZ_2\left(\frac{\tan\theta_3 + p\tan\theta_2}{p - \tan\theta_2\tan\theta_3}\right), \text{ where } p = Z_2/Z_3 \tag{2}$$

$$Z_{\text{in}} = Z_1\left(\frac{Z_L + jZ_1\tan\theta_1}{Z_1 + jZ_L\tan\theta_1}\right). \tag{3}$$

The fundamental and harmonic modes of the resonator are the frequencies at which the imaginary part of input admittance of the resonator equals zero.

Input admittance is given by $y_{\text{in}} = (1/Z_{\text{in}})$. By making the input admittance $y_{\text{in}} = 0$, the condition obtained is given in the following equation:

$$Z_1[p - \tan\theta_2\tan\theta_3] - Z_2[\tan\theta_3 + p\tan\theta_2]\tan\theta_1 = 0. \tag{4}$$

This condition in (4) gives a fundamental mode at $f_0 = 0.35$ GHz and harmonic at $f_1 = 1.8$ GHz. These can be viewed from the input impedance versus frequency plot in Fig. 3 for parameters $Z_1 = 84.13$, $Z_2 = 10.38$, $Z_3 = 84.13$, $\theta_1 = 2.96$, $\theta_2 = 1.238$, and $\theta_3 = 7.18$. From (4), it is visible that the modes of OSL-SCSIR depend on the four parameters, i.e., impedance ratio p, and lengths of each transmission line section θ_1, θ_2, and θ_3.

The variation in resonant frequency of the resonator with p, θ_1, and θ_3 is shown in Fig. 4. (Values are obtained from EM simulations in CST Microwave Studio software.) As the impedance ratio p increases, the resonant frequency shifts toward higher frequency, which is in conjuncture with the nature of stepped-impedance stubs. As the electrical lengths θ_1 and θ_3 increase, the resonant frequency shifts toward lower frequencies. Hence, according to the required resonant frequency, the parameters of the resonator have to be chosen.

III. Proposed Filter Design

The main goal is to design a compact bandpass filter at center frequency of 0.35 GHz for TETRA band applications with a fractional bandwidth (FBW) of 10%, return loss of greater than 20 dB, and a wide stopband at least up to $4.9f_0$. After the resonator dimensions are determined as per the center frequency of the specified filter, remaining dimensions are determined as follows.

A. Coupling Gaps

The type of coupling between the resonators depends upon coupling orientation in which they are coupled. In the proposed

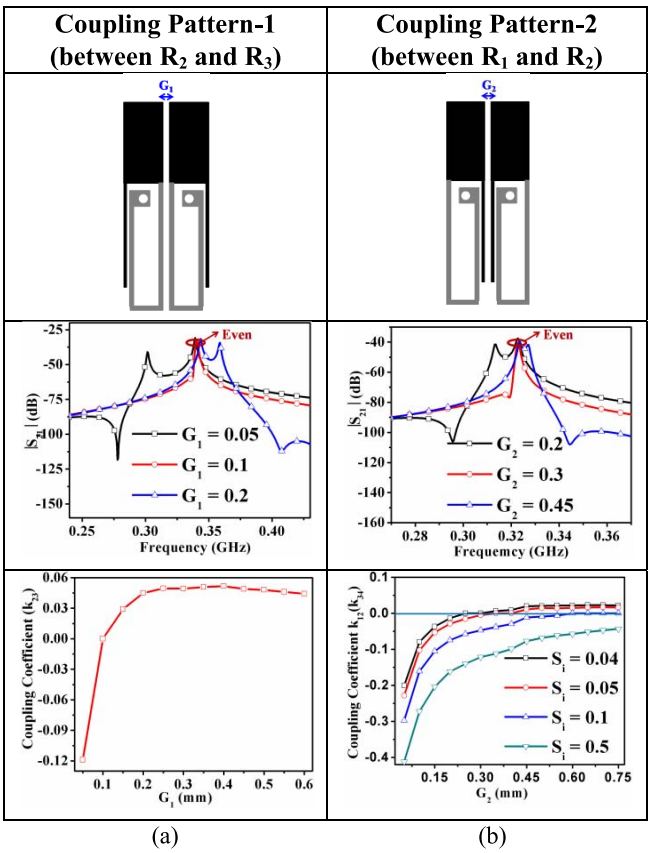

Fig. 5. Variation in coupling coefficient and modes of the coupling resonators. (a) R_2 and R_3. (b) R_1 and R_2.

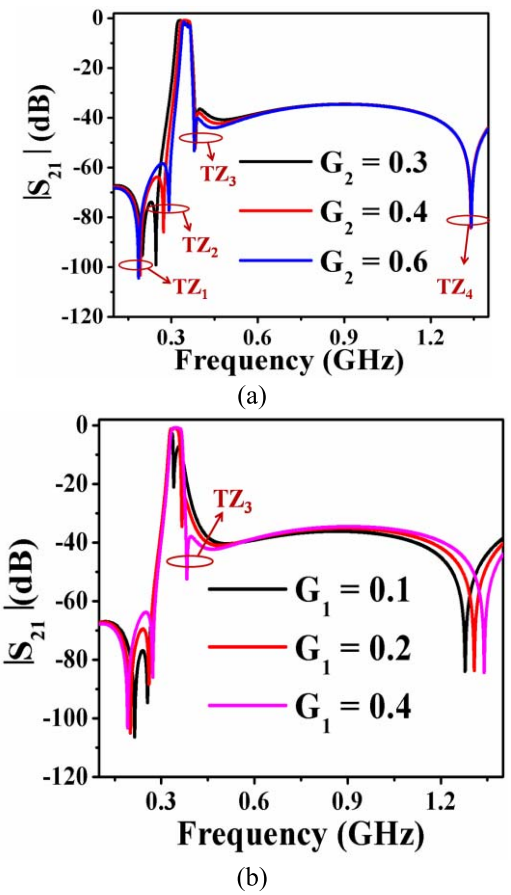

Fig. 6. Change in frequency response of the filter with (a) G_2 and (b) G_1.

filter shown in Fig. 1(a), two types of coupling orientations are used, which are shown in Fig. 5(a) and (b). In both orientations, dominant magnetic field is experienced at gray parts and dominant electric field is experienced at dark parts of the resonator. In Fig. 5(a), the coupling between R_2 and R_3, the frequency response variation with G_1 is shown. As the value of G_1 is increased, among the two modes, even mode is almost constant, while odd mode and the transmission zero shift to higher frequencies. The shift in the odd mode and transmission zero (TZ) (which is generated because of mixed coupling between these resonators as per [24]) position is due to the change in coupling between the resonators from dominant electric to dominant magnetic with change in G_1. As per (5) [24], when $f_{\text{odd}} > f_{\text{even}}$, $k_{23} > 0$ resembles dominant magnetic coupling, and when $f_{\text{odd}} < f_{\text{even}}$, $k_{23} < 0$ resembles dominant electric coupling. This can be verified from the coupling coefficient variation with space parameter G_1. It is clearly visible that the coupling coefficient starts with positive value and turns to negative value as G_1 increases. This explains that at smaller value of G_1, there exists mixed coupling between the resonators

$$k = \frac{f_{\text{odd}}^2 - f_{\text{even}}^2}{f_{\text{odd}}^2 + f_{\text{even}}^2}. \tag{5}$$

In a similar way, between R_1 and R_2 also, mixed coupling exists, which can be observed from the coupling coefficient and modes variation graphs shown in Fig. 5(b). As G_2 changes (with value of S_i fixed), the coupling coefficient changes from negative to positive value as shown in Fig. 5(b). Furthermore, the position of change in the sign of the coupling coefficient (k_{12}/k_{34}) increases as S_i increases. Thus, the value of the coupling coefficient between the resonators depends on two parameters, namely, G_2 and S_i.

This mixed coupling generates TZ, and the frequency of this TZ can be tuned by varying the mixed coupling coefficient between the resonators, i.e., by changing the gap between the resonators [24].

In Fig. 6(a), it can be seen that there exist four TZs, TZ_1–TZ_4. Among the four transmission zeros, TZ_2 is because of the mixed coupling between resonators R_1-R_2 and R_3-R_4. It is clearly visible that, except for TZ_2, remaining TZs are constant with respect to space between the resonators (G_2). From Fig. 6(b), it can be observed that as the gap between the resonators R_3-R_4 is changed, the frequency of TZ_3 changes. This clearly explains that the existence of TZ_3 is due to the presence of mixed coupling between the resonators. Therefore, the gap between the resonators is optimized according to the requirement of the TZs position around passband.

B. Input–Output Impedance Transformer Parameters

Once the resonator dimensions and gap between the parameters are obtained, the dimensions of input–output coupling ITs and coupling gaps are to be determined according to the requirement of quality factor, return loss, and bandwidth.

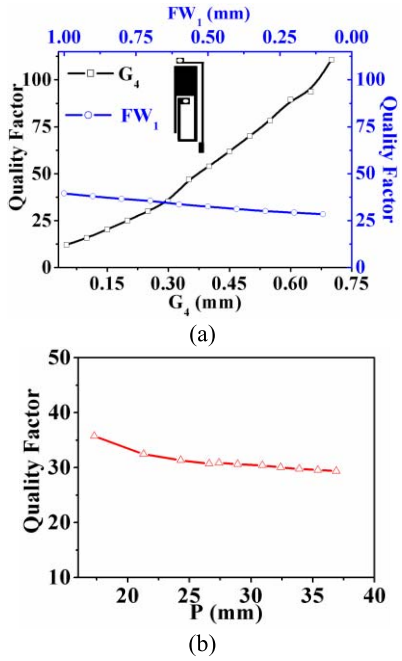

Fig. 7. (a) Change in EQF with G_4 and FW_1. (b) Change in EQF with P.

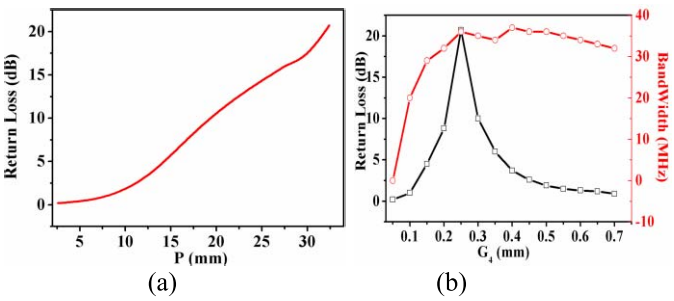

Fig. 8. (a) Variation in return loss of the filter response with parameter P. (b) Variation in return loss and bandwidth of the filter response with parameter G_4.

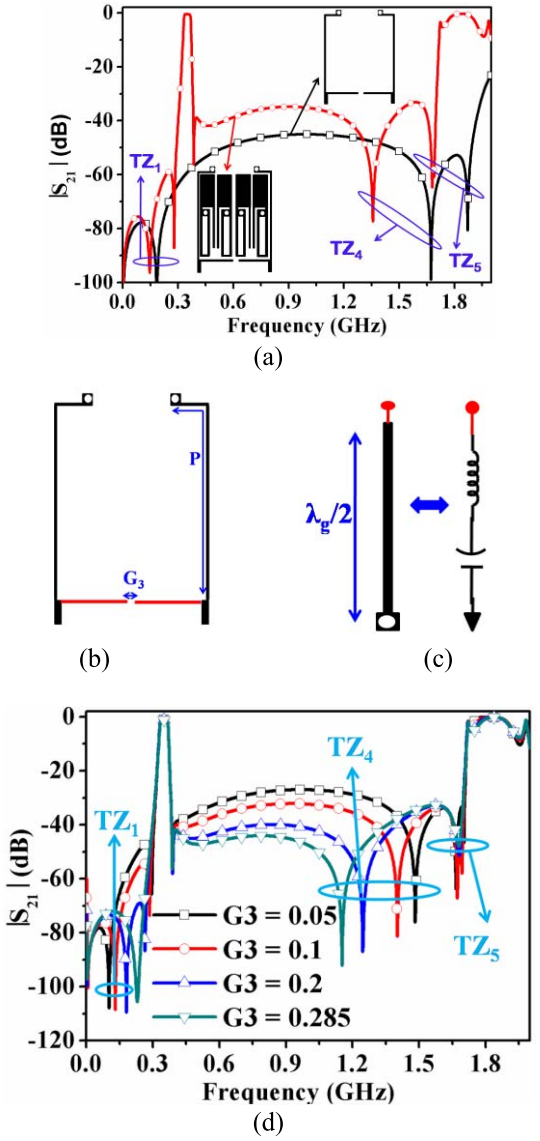

Fig. 9. (a) Frequency response of the total filter and only feedlines. (b) Layout of the feedlines structure. (c) Half-wavelength resonator and its lumped equivalent. (d) Change in frequency response of the filter with parameter G_3.

The external quality factor (EQF) (Q_{eff}), can be calculated from (6) taken from [25, Ch. 8]

$$Q_{\text{eff}} = \frac{\omega_0 \tau_{S_{11}}(\omega_0)}{4} \tag{6}$$

where τ_{S11} = group delay at resonant frequency of resonator, $\omega_0 = 2\pi f_0$, and f_0 is the self-resonant frequency of resonator. The change in Q_{eff} with input–output coupling gap between resonator and IT lines and length and width of IT lines is shown in Fig. 7. Fig. 7(a) shows that Q_{eff} increases with I/O coupling gap and with width of the IT lines. Q_{eff} is nearly constant with respect to length of the IT lines. Hence, the bandwidth of the filter can be tuned with the help of two parameters G_4 and FW_1.

From Fig. 8(a), it can be seen that as IT length increases, the return loss value increases. At $p = 32.4$, the return loss reaches 20 dB, which is as per design specifications of the filter. In Fig. 8(b), the change in bandwidth and return loss of the filter response with G_4 is shown. From this graph, it is visible that when $G_4 = 0.25$, the optimum value of bandwidth and return loss are achieved.

The TZ_1 and TZ_4 are due to the input–output feedline structure. From Fig. 9, the variation in the frequency response of the total filter and the frequency response with feedlines alone can be observed. First and fourth TZs are present even when all the resonators were removed; this proves that these TZs are due to the feedline structure. TZ_1 and TZ_4 are due to the coupling between source and load, which is because of the coupling between two open stubs (red in Fig. 9(a) with coupling gap G_3 in between) connected to the 50-Ω feedlines. In Fig. 9(d), a graph of change in frequency response of the filter with different coupling gaps (G_3) is shown, which depicts that the transmission zeros TZ_1 and TZ_4 vary with change in G_3 (without any change in the frequency of TZ_2, TZ_3, and TZ_5); at $G_3 = 0.285$, the transmission zero TZ_1 vanishes. This validates that the generation of TZ_1 and TZ_4 is generated by virtue of cross coupling between source and load through open stubs connected to the feedlines. The feedlines

TABLE I
COMPARISON OF THE PROPOSED WORK WITH REPORTED WORKS

Ref.	Technique	f_0/ FBW	I	R	N	HS	Size ($\lambda_g \times \lambda_g$)
[5]	**Coupled SIRs**	1.5/8.9	2.52	10.19	--	$10.6f_0$	0.336×0.252
[8]	**Stub loaded Open Loop Resonators**	1.46/9	--	> 17	5	$3.2f_0$	0.17×0.1
[10]	**Dual Mode Ring Resonator**	2.52/5.18	>1.5	>15	2	----	0.17×1.147
[11]	**Dual Mode Ring Resonator**	0.85/4.7	2.5	15	--	$< 2.5f_0$	0.167×0.087
[15]	**Mixed coupled SIRs**	3.5/8.5	1.2	> 20	3	$3.42f_0$	0.2×0.09
[19]	**Hybrid Inter-digital Resonators**	2.18/5.3	1.6	> 18	3	$< 2f_0$	0.157×0.127
[21]	**Triangular stub resonator**	0.33/20.5	< 0.65	20.5	3	$< 4.5f_0$	0.12×0.13
[22]	**Parallel feeding Technique**	8.7/18.4	< 2.4	16.5	4	$< 2.2f_0$	0.42×0.2
[23]	**Shunt serial and parallel resonators**	2.45/10	>0.79	22	4	--	0.92×0.345
This work	**Mixed coupled OSL-SCSIR**	**0.34/10**	**1.2**	**19**	**5**	**4.9 f_0 (27.5 dB)**	**0.078×0.082**

ϵ_r = permittivity; f_0 = centre frequency (GHz); FBW = -3 dB fractional bandwidth (%); I = Insertion Loss (dB); R = Return Loss (dB); S = N=No. of. Transmission Zeros; HS = Harmonic suppression (20 dB level)

act as half-wavelength resonator at f_{TZ5}; at this frequency, it acts as a series L–C resonator as in Fig. 9(c). Therefore, at f_{TZ5} it generates a transmission zero. This is the reason for not having variation in TZ5 position in Fig. 9(d) as it totally depends on the length of the feedlines only.

In summary, the design procedure of the proposed bandpass filter is given in the following.

1) The resonator dimensions and stub lengths are to be determined based on the required operating frequency of the filter from design graphs as shown in Fig. 4 obtained from (4).
2) The orientation of the coupled resonators is set in such a way that mixed coupling exists between them. The transmission zero generated because of the mixed coupling between the resonators is tuned to place them near the passband by varying the gap between the resonators.
3) Once the resonator dimensions and the coupling gaps are obtained, the dimensions of the ITs and input–output coupling gaps are to be obtained depending on the values of bandwidth and return loss requirement. The flowchart for the design procedure is shown in Fig. 10.

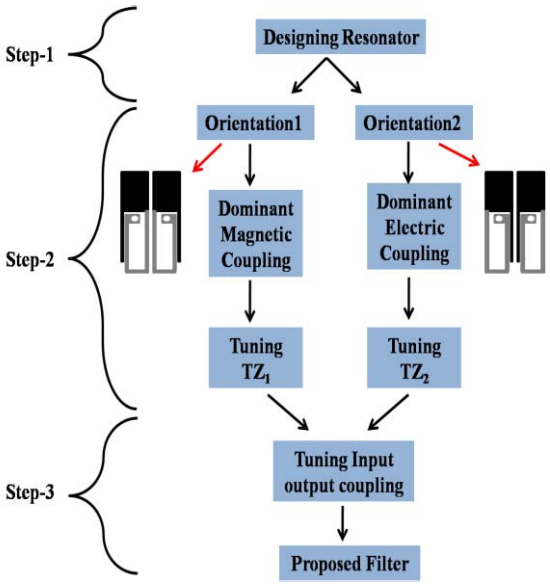

Fig. 10. Flowchart for the process to design proposed bandpass filter.

IV. RESULTS AND DISCUSSION

The optimized parameters of the filter used for experimentation are W_{a1}5.8, $W_{a2} = 5.65$, $W_{b1} = 0.45$, $W_{b2} = 0.3$, $W_{c1} = 0.3$, $W_{c2} = 0.4$, $W_{d1} = 0.2$, $W_{d2} = 0.2$, $W_{e1} = 0.3$, $W_{e2} = 0.2$, $L_{a1} = 12$, $L_{a2} = 12$, $L_{b1} = 13.5$, $L_{b2} = 13.5$, $L_{c1} = 30.25$, $L_{c2} = 30.25$, $P = 31.5$, $S_1 = 0.5$, $S_2 = 0.5$, $G_1 = 0.4$, $G_2 = 0.4$, $G_3 = 0.25$, $G_4 = 0.3$, $F_{w1} = 0.3$, $F_{L1} = 11.55$, and $F_{50} = 1.2$ (units: mm). Fabrication of the filter is done by manual photolithography etching process. The experimental (measurement done with vector network analyzer Agilent E5071C) and simulation results of the proposed filter are compared in Fig. 11(a). The inset picture in Fig. 11(b)

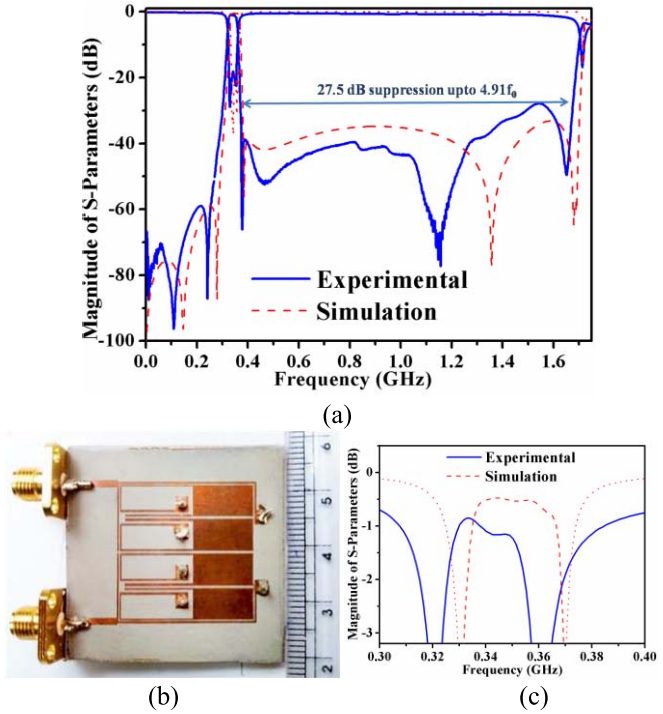

Fig. 11. (a) Comparison of the experimental and simulation results. (b) Image of the proposed filter fabricated prototype. (c) Zoomed-in view of passband response of the filter.

shows the fabricated structure. Fig. 11(c) shows that the filter operates at a center frequency of 0.3405 GHz having an FBW of 10%. The TZs are generated at 0.12, 0.25, 0.375, 1.15, and 1.65 GHz. The maximum insertion and minimum return loss are obtained as 1.2 and 19 dB. The stopband is extended up to 4.91 f_0 (f_0 is the center frequency) with suppression level of 27.5 dB. The proposed filter has the asset of high selectivity, which can be quantified by the parameter $BW_{(3dB)}/BW_{(20dB)}$ and is equal to 0.609. The slight variation in the positions of transmission zeros can be attributed to the fabrication tolerances of thin microstrip lines and of vias. The proposed work is compared with recently reported works in Table I. The superiority of the work is clearly established from the tabulated results.

V. Conclusion

A miniaturized selective bandpass filter for TETRA band applications is proposed in this paper. The filter is constructed with the help of a compact resonator OSLSC-SIR. For achieving good selectivity, three transmission zeros are realized around passband with the help of EM coupling between resonators and source load cross coupling. A wide stopband with good suppression is obtained with the help of two transmission zeros in stopband. The filter is designed, analyzed, and experimentally verified.

References

[1] S. B. Cohn, "Parallel-coupled transmission-line-resonator filters," *IRE Trans. Microw. Theory Techn.*, vol. MTT-6, no. 2, pp. 223–231, Apr. 1958.

[2] T. Lopetegi *et al.*, "New microstrip 'wiggly-line' filters with spurious passband suppression," *IEEE Trans. Microw. Theory Techn.*, vol. 49, no. 9, pp. 1593–1598, Sep. 2001.

[3] J. T. Kuo and E. Shih, "Microstrip stepped impedance resonator bandpass filter with an extended optimal rejection bandwidth," *IEEE Trans. Microw. Theory Techn.*, vol. 51, no. 5, pp. 1554–1559, May 2003.

[4] I. K. Kim *et al.*, "Fractal-shaped microstrip coupled-line bandpass filters for suppression of second harmonic," *IEEE Trans. Microw. Theory Techn.*, vol. 53, no. 9, pp. 2943–2948, Sep. 2005.

[5] C. H. Kim and K. Chang, "Wide-stopband bandpass filters using asymmetric stepped-impedance resonators," *IEEE Microw. Wireless Compon. Lett.*, vol. 23, no. 2, pp. 69–71, Feb. 2013.

[6] J.-T. Kuo, M.-J. Maa, and P.-H. Lu, "A microstrip elliptic function filter with compact miniaturized hairpin resonators," *IEEE Microw. Guided Wave Lett.*, vol. 10, no. 3, pp. 94–95, Mar. 2000.

[7] J.-S. Hong and M. J. Lancaster, "Design of highly selective microstrip bandpass filters with a single pair of attenuation poles at finite frequencies," *IEEE Trans. Microw. Theory Techn.*, vol. 48, no. 7, pp. 1098–1107, Jul. 2000.

[8] N. Kumar and Y. K. Singh, "Compact stub-loaded open-loop BPF with enhanced stopband by introducing extra transmission zeros," *Electron. Lett.*, vol. 51, no. 2, pp. 164–166, 2015.

[9] A. Gorur, "A novel dual-mode bandpass filter with wide stopband using the properties of microstrip open-loop resonator," *IEEE Microw. Wireless Compon. Lett.*, vol. 12, no. 10, pp. 386–388, Oct. 2002.

[10] T. W. Lin, J. T. Kuo, and S. J. Chung, "Dual-mode ring resonator bandpass filter with asymmetric inductive coupling and its miniaturization," *IEEE Trans. Microw. Theory Techn.*, vol. 60, no. 9, pp. 2808–2814, Sep. 2012.

[11] H.-W. Hsu, C.-H. Lai, and T.-G. Ma, "A miniaturized dual-mode ring bandpass filter," *IEEE Microw. Wireless Compon. Lett.*, vol. 20, no. 10, pp. 542–544, Oct. 2010.

[12] G. Jang and S. Kahng, "Compact metamaterial zeroth-order resonator bandpass filter for a UHF band and its stopband improvement by transmission zeros," *Microw., Antennas Propag.*, vol. 5, no. 10, pp. 1175–1181, Jul. 2011.

[13] H. Zhang and K. J. Chen, "A tri-section stepped-impedance resonator for cross-coupled bandpass filters," *IEEE Microw. Wireless Compon. Lett.*, vol. 15, no. 6, pp. 401–403, Jun. 2005.

[14] R.-J. Mao, X.-H. Tang, L. Wang, and G.-H. Du, "Miniaturized hexagonal stepped-impedance resonators and their applications to filters," *IEEE Trans. Microw. Theory Techn.*, vol. 56, no. 2, pp. 440–448, Feb. 2008.

[15] F. Zhu, W. Hong, J.-X. Chen, and K. Wu, "Quarter-wavelength stepped-impedance resonator filter with mixed electric and magnetic coupling," *IEEE Microw. Wireless Compon. Lett.*, vol. 24, no. 2, pp. 90–92, Feb. 2014.

[16] Y. S. Won, K. U. Bae, and N. H. Myung, "Design method for bandpass filter with enhanced stopband rejection using spiral SIRs," *Electron. Lett.*, vol. 48, no. 17, pp. 1067–1068, Aug. 2012.

[17] J. Zhou, M. J. Lancaster, and F. Huang, "HTS coplanar meander-line resonator filters with a suppressed slot-line mode," *IEEE Trans. Appl. Supercond.*, vol. 14, no. 1, pp. 28–32, Mar. 2004.

[18] T. Yang, M. Tamura, and T. Itoh, "Compact hybrid resonator with series and shunt resonances used in miniaturized filters and balun filters," *IEEE Trans. Microw. Theory Techn.*, vol. 58, no. 2, pp. 390–402, Feb. 2010.

[19] B. F. Zong, G. M. Wang, J. G. Liang, and C. Zhou, "Compact bandpass filter with two tunable transmission zeros using hybrid resonators," *IEEE Microw. Wireless Compon. Lett.*, vol. 25, no. 2, pp. 88–90, Feb. 2015.

[20] W. Qin and Q. Xue, "Complementary compact microstrip resonant cell and its applications to microwave single- and dual-band bandpass filters," *IEEE Trans. Microw. Theory Techn.*, vol. 61, no. 2, pp. 773–781, Feb. 2013.

[21] Z. He, Z. Shao, and C. J. You, "Parallel feed bandpass filter with high selectivity and wide stopband," *Electron. Lett.*, vol. 52, no. 10, pp. 844–846, 2016.

[22] V. K. Killamsetty and B. Mukherjee, "Compact wideband bandpass filter for TETRA band applications," *IEEE Microw. Wireless Compon. Lett.*, vol. 27, no. 7, pp. 630–632, Jul. 2017.

[23] S. Chen, L.-F. Shi, G.-X. Liu, and J.-H. Xun, "An alternate circuit for narrow-bandpass elliptic microstrip filter design," *IEEE Microw. Wireless Compon. Lett.*, vol. 27, no. 7, pp. 624–626, Jul. 2017.

[24] Q.-X. Chu and H. Wang, "A compact open-loop filter with mixed electric and magnetic coupling," *IEEE Trans. Microw. Theory Techn.*, vol. 56, no. 2, pp. 431–439, Feb. 2008.

[25] J.-S. G. Hong and M. J. Lancaster, *Microstrip Filters for RF/Microwave Applications*. New York, NY, USA: Wiley, 2001.

Vinay Kumar Killamsetty (S'16) received the B.Tech. degree in electronics and communication engineering from Jawaharlal Nehru Technological University, Kakinada, India, and the M.Tech. degree in radar and microwave engineering from the Department of Electronics and Communication, Andhra University, Visakhapatnam, India. He is currently pursuing the Ph.D. degree with the Department of Electronics and Communication Engineering, Indian Institute of Information Technology, Design and Manufacturing, Jabalpur, India.

He has authored and coauthored nine articles in international peer-reviewed journals. His current research interests include planar filters, UWB antennas, meta-materials, dielectric resonator antennas, and plasmonic filters for wireless communication.

Biswajeet Mukherjee (M'14–SM'17) received the B.Tech. degree from the Electronics and Communication Engineering Department, Indraprastha University, Delhi, India, the M.Tech. degree in microwave electronics from the Department of Electronic Science, University of Delhi, New Delhi, India, and the Ph.D. degree from IIT Bombay, Mumbai, India.

In 2014, he joined the Department of Electronics and Communication Engineering, Indian Institute of Information Technology, Design and Manufacturing (IIITDM), Jabalpur, India, as an Assistant Professor. He has authored or coauthored over 40 research articles in international peer-reviewed journals and conferences. His research interests include microwave engineering, such as dielectric resonator antenna (DRA), filters, and metamaterials. His current research interests include dielectric resonators, antennas, MIC, monolithic microwave integrated circuit, and computational electromagnetics in finite-difference time domain.

Dr. Mukherjee received the Departmental Fellowship during his M.Tech. degree and also the Fellowship for training of Young Scientist from MAPCOST, Government of Madhya Pradesh, India, for pursuing research in the field of DRA and EBG. He was a recipient of the Young Scientist Award at URSI GASS 2014 and the IEI Young Engineering Award for 2016 in Electronics and Telecommunication Engineering Division. He actively involved in IEEE activities as an IIITDM Jabalpur Student Branch Counselor.